Measured dipole expansion of discrete relaxations to represent the electromagnetic induction response of buried metal targets

Waymond R. Scott, Jr.[*] and Gregg D. Larson[†]
[*]School of Elec. and Comp. Eng., Georgia Institute of Technology, Atlanta, GA, USA 30332-0250
[†]Woodruff School of Mech. Eng., Georgia Institute of Technology, Atlanta, GA, USA 30332-0405

ABSTRACT

Broadband electromagnetic induction (EMI) sensors have been shown to be able to reduce false alarm rates and increase the probability of detecting landmines. To aid in the development of these sensors and associated detection algorithms, a testing facility and inversion technique have been developed to characterize the response of typical targets and clutter objects as a function of orientation and frequency. The models are simple sets of magnetic dipoles with discrete relaxation frequencies. Results will be presented for a range of targets such as shell casings, wire loops, and landmines. It is envisioned that the models derived in this work will be utilized to reduce false alarm rates and increase the probability of detection for EMI sensors through improvements in both the hardware and the processing algorithms used to detect and discriminate buried targets.

Keywords: Electromagnetic induction, EMI, landmine detection, sensor, testing

1. INTRODUCTION

Simple electromagnetic induction (EMI) sensors are capable of detecting most landmines; however, they will also detect every buried metal object such as bottle tops, nails, shrapnel, bullets, etc. This results in an unacceptable false alarm rate. This is even more problematic for the detection of low-metal anti-personnel landmines as they are extremely difficult to distinguish from clutter using a simple EMI sensor. However, advanced EMI sensors that use a broad range of frequencies or a broad range of measurement times along with advanced signal processing have been shown to be capable of discriminating between buried landmines and many types of buried metal clutter [1-6]. The broadband responses of many targets are relatively invariant to burial depth; however, the responses of some objects vary when they are tilted at odd angles, which could cause missed detections. To aid in the development of the EMI sensors and associated detection algorithms, a testing facility and inversion technique have been developed to characterize the response of typical targets and clutter objects with respect to location, orientation, and frequency. The data from these measurements will be used to study the response of the targets and develop models that are valid for any orientation of the object. Similar measurements in the field would be very difficult to perform due to the difficulty of accurately placing and rotating the target. It is difficult to analytically or numerically predict the response of many of these objects with accuracy due to uncertainties in the material parameters and geometry of the metal components in the objects. Most of these objects can be modeled as simple sets of magnetic dipoles with discrete relaxation frequencies. It is envisioned that the models derived in this work will be utilized to reduce false alarm rates and increase the probability of detection for EMI sensors through improvements in both the hardware and the processing algorithms used to detect and discriminate buried targets.

In this paper, the measurement system is presented in section 2, the model used to represent the targets is presented in section 3, the method for inverting the measured data to get the parameters for the model is presented in section 4, and representative results are presented in section 5.

[*] E-mail: waymond.scott@ece.gatech.edu, Tel: 404-894-3048
[†] E-mail: gregg.larson@me.gatech.edu, Tel: 404-894-6026

2. MEASUREMENT SYSTEM

A laboratory positioner was developed with three automated translational stages (*x*, *y*, and *z*), two automated rotational stages (yaw and pitch), and one manually-adjusted rotational stage (roll, not labeled) as indicated in Fig. 1 [7]. An EMI sensor array [8] is shown in Fig. 1b with the three-loop target. This system is used to measure the response of targets in a three-dimensional region as a function of angular orientation. Other typical targets include shell casings, ball bearings, coplanar wire coils, and landmines.

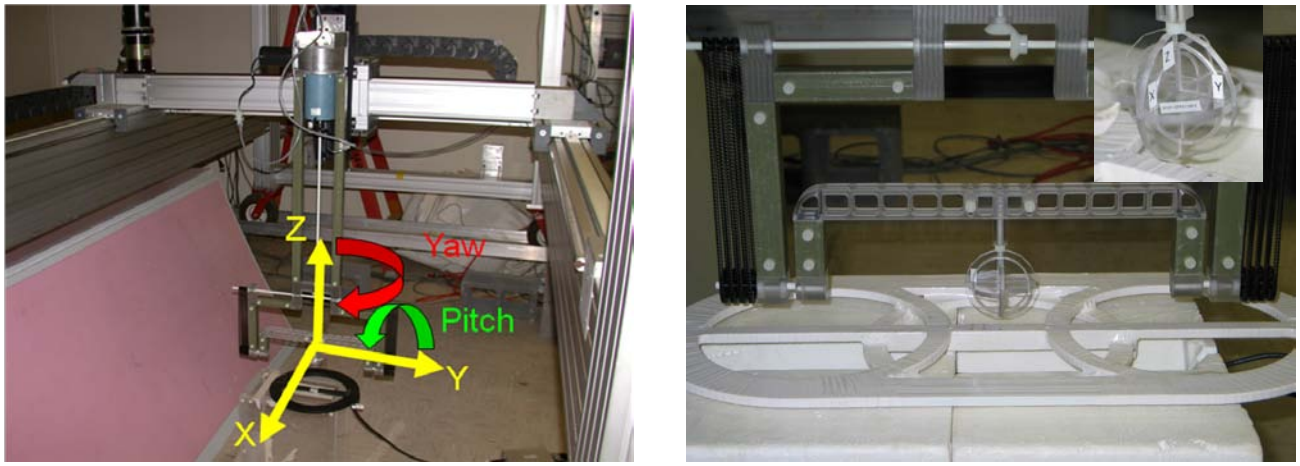

a) b)

Fig. 1. Experimental measurement facility for EMI target characterization: a) Single EMI sensor head with automated translational (x, y, and z) and rotational (yaw about z and pitch about y) axes labeled, manual rotational axis (roll about x) unlabeled; b) EMI sensor head array with three-loop target (inset).

3. MODEL

A simple dipole model is developed to predict the response of the EMI systems shown in figure 1 to a target that is being tested in the system as a function of its position and orientation.

3.1. Magnetic Polarizability of a Target

When a target is placed in a time-varying magnetic field, magnetic moments are induced due to two effects: the magnetic permeability of the target and the electrical conductivity that allows the induction of current. If the target is electrically small, the magnetic moments can be expressed in terms of the equivalent magnetic dipole moment, m. The dipole moment can be calculated from the magnetic polarizability, **M**, when the exciting field $\mathbf{H}_T$ is relatively constant over the extent of the object: $\mathrm{m} = \mathbf{M}\mathrm{H}_T$. A target will often have multiple relaxations and will have a corresponding tensor for each relaxation that contains the orientation/symmetry information for the relaxation. The magnetization for such a target can be written as the sum [2]:

$$\mathbf{M}(\omega) = T_0\mathbf{T}_0 - \sum_k T_k\left(\frac{j\omega/\zeta_k}{1+j\omega/\zeta_k}\right)\mathbf{T}_k \tag{1}$$

where T_k is a real constant, ζ_k is the relaxation frequency, and $\mathbf{T}_k$ is a real, symmetric, second rank tensor. The first term is due to the bulk magnetic permeability of the target, which is assumed to be frequency independent, and the second term is due to the currents induced in the target. The tensor $\mathbf{T}_k$ results from the symmetry of the current path for the k^{th} relaxation and can be expressed as sum of (projection matrices) simple dipoles:

$$T_k \mathbf{T}_k = \sum_n M_{kn} \mathbf{n}_{kn} \mathbf{n}_{kn}^T = \sum_n M_{kn} \begin{bmatrix} \mathrm{n}_{x,kn} \\ \mathrm{n}_{y,kn} \\ \mathrm{n}_{z,kn} \end{bmatrix} \begin{bmatrix} \mathrm{n}_{x,kn} & \mathrm{n}_{y,kn} & \mathrm{n}_{z,kn} \end{bmatrix} \tag{2}$$

where M_{kn} is a positive real constant and $\mathbf{n}_{kn}$ are orthogonal unit vectors representing the axis of the n^{th} dipole for the k^{th} relaxation frequency. As an example, a target that consists of three orthogonal loops of copper wire, as in Fig. 1b, was constructed with the parameters shown in Table I. The magnetization of this target is

$$\mathbf{M}(\omega) = -M_x \left(\frac{j\omega/\zeta_x}{1 + j\omega/\zeta_x} \right) \begin{bmatrix} 1 & 0 & 0 \\ 0 & 0 & 0 \\ 0 & 0 & 0 \end{bmatrix} - M_y \left(\frac{j\omega/\zeta_y}{1 + j\omega/\zeta_y} \right) \begin{bmatrix} 0 & 0 & 0 \\ 0 & 1 & 0 \\ 0 & 0 & 0 \end{bmatrix} - M_z \left(\frac{j\omega/\zeta_z}{1 + j\omega/\zeta_z} \right) \begin{bmatrix} 0 & 0 & 0 \\ 0 & 0 & 0 \\ 0 & 0 & 1 \end{bmatrix} \tag{3}$$

where $M_{\mathrm{k}} = \mu_o A_k^2 / L_k$, $\zeta_k = 2\pi f_{rk}$, A_k are the areas of the loops and, L_k are the self inductances of the loops with $k = x, y, z$.

Table I. Parameters for the three-loop target.

Loop Parameters			Theoretical Model Parameters		Measured Model Parameters	
Orientation	Diameter (cm)	Wire Gauge (AWG)	Magnetization $\mathrm{M_k} * 10^6$ ($\mathrm{m^3}$)	Relaxation Freq. (kHz)	Magnetization $\mathrm{M_k} * 10^6$ ($\mathrm{m^3}$)	Relaxation Freq. (kHz)
X	5	36	24.5	172	24.4	175
Y	4	30	14.7	50.2	14.7	52.6
Z	3	22	8.0	10.1	7.6	10.5

3.2. EMI System

Consider the example EMI system shown in figure 2 that consists of transmit and receive coils which interact with a target. Here $\mathbf{H}_T$ is the field at the target generated by the transmit coil when the coil is driven with the current I_T, and $\mathbf{m}$ is the dipole moment induced on the target. It can be shown by using reciprocity that the received voltage due to the target is [9, 10]:

$$V_R = \frac{j\omega\mu}{I_R} \mathbf{H}_R^T \mathbf{m} = \frac{j\omega\mu}{I_R} \mathbf{H}_R^T \mathbf{M} \mathbf{H}_T \tag{4}$$

where $\mathbf{H}_R$ is the magnetic field generated with the receiving loop driven with the current I_R. Note that $\mathbf{H}_T$, $\mathbf{H}_R$, and $\mathbf{m}$ can be, and are likely to be, in different directions. The received voltage is compared to a reference voltage to obtain the response $\mathcal{R}$ of the system:

$$\mathcal{R} = \frac{V_R}{V_X} = \frac{\mu}{L_X I_T I_R} \mathbf{H}_R^T \mathbf{M} \mathbf{H}_T \tag{5}$$

where $V_X = j\omega L_X I_T$ is the reference voltage from a reference transformer with mutual inductance L_X which is also driven by transmit current I_T. The response of the system when the target is rotated by the Euler angles α, β, and γ can be written as

$$\mathcal{R} = \frac{\mu}{L_X I_T I_R}\mathbf{H}_R^T \mathbf{M}_R \mathbf{H}_T = \frac{\mu}{L_X I_T I_R}\mathbf{H}_R^T \mathbf{R}^T(\alpha,\beta,\gamma)\mathbf{M}_R \mathbf{R}(\alpha,\beta,\gamma)\mathbf{H}_T$$
$$= \frac{\mu}{L_X I_T I_R}\mathbf{H}_R^T \mathbf{R}^T(\alpha,\beta,\gamma)\left\{T_0\mathbf{T}_0 - \sum_k T_k\left(\frac{j\omega/\zeta_k}{1+j\omega/\zeta_k}\right)\mathbf{T}_k\right\}\mathbf{R}(\alpha,\beta,\gamma)\mathbf{H}_T \quad (6)$$

where R is a rotation matrix[11]. The angle α is the yaw angle, β is the pitch angle, and γ is the roll angle; the yaw and pitch angles are indicated in figure 1. The magnetic fields $\mathbf{H}_T(x, y, z)$ and $\mathbf{H}_R(x, y, z)$ are calculated as a function of position by direct application of the Bio-Savart law from the geometry of the wires in the coils.

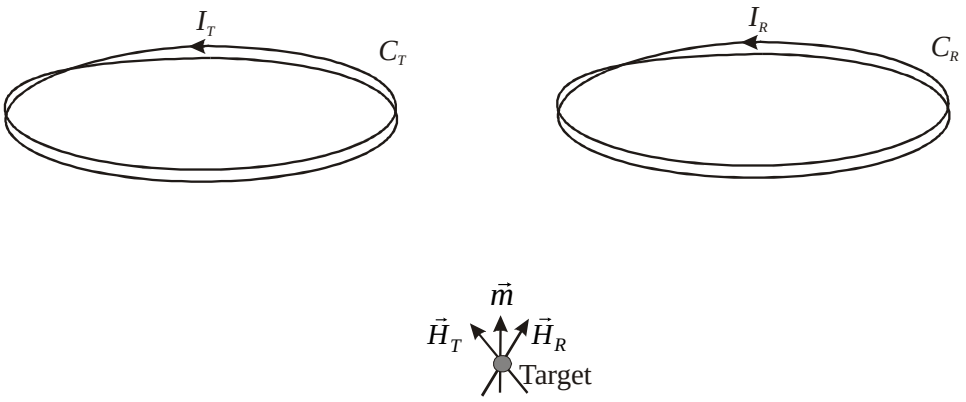

Figure 2a. Diagram of EMI system used with the reciprocity relation with both the transmit and the receive coils driven.

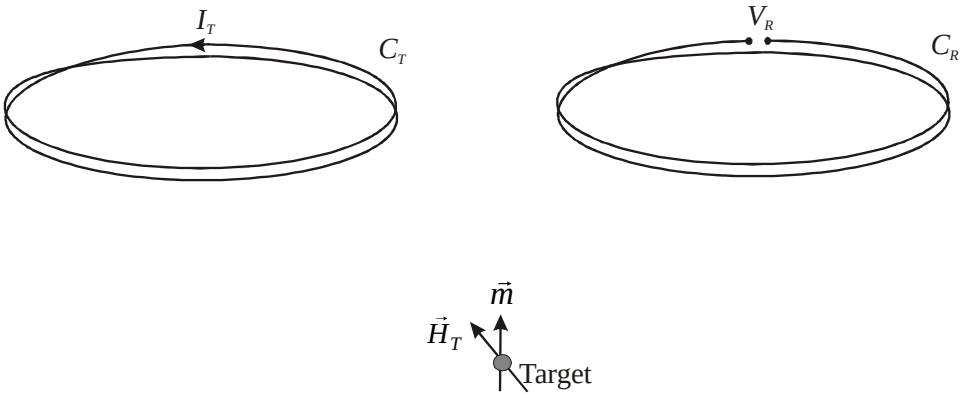

Figure 2b. Diagram of EMI system as it is physically configured with the transmit coil driven and receive coil used a receiver.

4. ESTIMATION OF TARGET PARAMETERS

In a typical measurement, the response $\mathcal{R}$ is measured as a function of position and orientation, and in this section, a method for inverting the measurement to obtain the model parameters is presented. Direct fitting of the parameters in equations 2 and 6 is difficult because of the non-linear relationship between the relaxation frequencies ζ_k and the vectors

$\mathbf{n}_{kn}$ with the response. The non-linear relation for ζ_k is dealt with using the procedure described in [12]. The non-linear relation for $\mathbf{n}_{kn}$ is dealt with by using an alternate expansion of $\mathbf{T}_k$. Here, the tensor $\mathbf{T}_k$ is expanded in a set of basis tensors $\mathcal{T}_k$ which span the allowable range of $\mathbf{T}_k$:

$$T_k \mathbf{T}_k = \sum_n M_{kn} \mathcal{T}_n = \sum_n M_{kn} \begin{bmatrix} \mathcal{T}_{n,11} & \mathcal{T}_{n,12} & \mathcal{T}_{n,13} \\ \mathcal{T}_{n,21} & \mathcal{T}_{n,22} & \mathcal{T}_{n,23} \\ \mathcal{T}_{n,31} & \mathcal{T}_{n,32} & \mathcal{T}_{n,33} \end{bmatrix}. \tag{7}$$

This expansion allows for solution of the parameters M_{kn} using a linear least-squares approximation procedure. However, there are two disadvantages of this expansion for an arbitrary target: first, the coefficients M_{kn} are no longer guaranteed to be positive, and second, more terms will be required. Up to six basis tensors can be required for a general target with an arbitrary initial orientation. Fortunately, most targets of interest have symmetry that negates these disadvantages. For this paper, three types of expansions will be considered. First, all targets can be oriented so that is $\mathbf{T}_k$ diagonal [11]. It can also be shown that $\mathbf{T}_k$ is diagonal for certain targets with symmetries about the coordinate axes[13]. The three loop target shown in figure 2b is an example of a target with this symmetry. For these targets, $\mathbf{T}_k$ is expanded as

$$T_k \mathbf{T}_k = M_{k,xx} \mathcal{T}_{xx} + M_{k,yy} \mathcal{T}_{yy} + M_{k,zz} \mathcal{T}_{zz} = M_{k,xx} \begin{bmatrix} 1 & 0 & 0 \\ 0 & 0 & 0 \\ 0 & 0 & 0 \end{bmatrix} + M_{k,yy} \begin{bmatrix} 0 & 0 & 0 \\ 0 & 1 & 0 \\ 0 & 0 & 0 \end{bmatrix} + M_{k,zz} \begin{bmatrix} 0 & 0 & 0 \\ 0 & 0 & 0 \\ 0 & 0 & 1 \end{bmatrix}. \tag{8}$$

Second, some targets have additional symmetry about the z-axis which can be used to further simply the expansion:

$$T_k \mathbf{T}_k = M_{k,cy} \mathcal{T}_{cy} + M_{k,zz} \mathcal{T}_{zz} = M_{k,cy} \begin{bmatrix} 1 & 0 & 0 \\ 0 & 1 & 0 \\ 0 & 0 & 0 \end{bmatrix} + M_{k,zz} \begin{bmatrix} 0 & 0 & 0 \\ 0 & 0 & 0 \\ 0 & 0 & 1 \end{bmatrix}. \tag{9}$$

A right regular polyhedral cylinder about the *z*-axis, a penny, and a rifle cartridge are examples of objects with this type of symmetry. Third, objects with even more summery like a sphere, a cube, a regular tetrahedron, etc. will only require one term in the expansion:

$$T_k \mathbf{T}_k = M_k \mathcal{T}_{sp} = M_k \begin{bmatrix} 1 & 0 & 0 \\ 0 & 1 & 0 \\ 0 & 0 & 1 \end{bmatrix}. \tag{10}$$

In all of these expansions (8), (9), and (10), the coefficients are positive since they are aligned with the physical dipoles.

A zero-mean down-track filter is applied to the measured response to lessen the effects of positional errors in the *x* direction, to increase the signal to noise ratio, to help mitigate the response to the positioning system, and to mostly remove the direct coupling between the transmit and receive coils[8]:

$$\mathcal{R}_F(\omega, x, y, z, \alpha, \beta, \gamma) = \sum_g F(x_g) \mathcal{R}(\omega, x_g + x, y, z, \alpha, \beta, \gamma) \tag{11}$$

where F is the down-track filter described in [8]. The filtered response is obtained at the discrete observations O_p by combing equations (6) and (7):

$$\mathcal{R}_F(O_p) = \frac{\mu}{L_X I_T I_R} \left\{ \sum_n M_{0n} \mathbf{P}_{pn} - \sum_k \left[\left(\frac{j\omega_p / \zeta_k}{1 + j\omega_p / \zeta_k} \right) \sum_n M_{kn} \mathbf{P}_{pn} \right] \right\} \tag{12}$$

where ω_p is the frequency at the p^{th} observation. $\mathbf{P}_{pn}$ contains the filtering, the projections of the tensors on the fields and the rotation matrices:

$$\mathbf{P}_{pn} = \sum_g F(x_g)\mathbf{H}_R^T(x_g + x_p, y_p, z_p)\mathbf{R}^T(\alpha_p, \beta_p, \gamma_p)\boldsymbol{\mathcal{T}}_n\mathbf{R}(\alpha_p, \beta_p, \gamma_p)\mathbf{H}_T(x_g + x_p, y_p, z_p) \tag{13}$$

where x_p, y_p, z_p, α_p, β_p, and γ_p are the locations/orientations at the p^{th} observation. The values of ζ_k are determined in this paper by computing the discrete spectrum of relaxation frequencies (DSRF) as described in [12] on a response that is averaged over all the discrete observations O_p. The sign of the responses are adjusted before averaging to ensure that the averaged response has a non-negative spectrum. The response is rewritten in a matrix equation for each location/orientation:

$$\begin{bmatrix} \mathcal{R}_F(O_p) \\ \mathcal{R}_F(O_p) \\ \mathcal{R}_F(O_p) \\ \vdots \\ \mathcal{R}_F(O_p) \end{bmatrix} = \begin{bmatrix} \mathbf{P}_{11} & \mathbf{P}_{12} & \cdots & \mathbf{P}_{1N} & \mathbf{P}_{11}\left(\frac{j\omega_1/\zeta_1}{1+j\omega_1/\zeta_1}\right) & \mathbf{P}_{12}\left(\frac{j\omega_1/\zeta_1}{1+j\omega_1/\zeta_1}\right) & \cdots & \mathbf{P}_{1N}\left(\frac{j\omega_1/\zeta_1}{1+j\omega_1/\zeta_1}\right) & \cdots & \mathbf{P}_{11}\left(\frac{j\omega_1/\zeta_K}{1+j\omega_1/\zeta_K}\right) & \cdots & \mathbf{P}_{1N}\left(\frac{j\omega_1/\zeta_K}{1+j\omega_1/\zeta_K}\right) \\ \mathbf{P}_{21} & \mathbf{P}_{22} & \cdots & \mathbf{P}_{2N} & \mathbf{P}_{21}\left(\frac{j\omega_2/\zeta_1}{1+j\omega_2/\zeta_1}\right) & \mathbf{P}_{22}\left(\frac{j\omega_2/\zeta_1}{1+j\omega_2/\zeta_1}\right) & \cdots & \mathbf{P}_{2N}\left(\frac{j\omega_2/\zeta_1}{1+j\omega_2/\zeta_1}\right) & \cdots & \mathbf{P}_{21}\left(\frac{j\omega_2/\zeta_K}{1+j\omega_2/\zeta_K}\right) & \cdots & \mathbf{P}_{2N}\left(\frac{j\omega_2/\zeta_K}{1+j\omega_2/\zeta_K}\right) \\ \mathbf{P}_{31} & \mathbf{P}_{32} & \cdots & \mathbf{P}_{3N} & \mathbf{P}_{31}\left(\frac{j\omega_3/\zeta_1}{1+j\omega_3/\zeta_1}\right) & \mathbf{P}_{32}\left(\frac{j\omega_3/\zeta_1}{1+j\omega_3/\zeta_1}\right) & \cdots & \mathbf{P}_{3N}\left(\frac{j\omega_3/\zeta_1}{1+j\omega_3/\zeta_1}\right) & \cdots & \mathbf{P}_{31}\left(\frac{j\omega_3/\zeta_K}{1+j\omega_3/\zeta_K}\right) & \cdots & \mathbf{P}_{3N}\left(\frac{j\omega_3/\zeta_K}{1+j\omega_3/\zeta_K}\right) \\ \vdots & \vdots & \vdots & \vdots & \vdots & \vdots & & \vdots & & \vdots & & \vdots \\ \mathbf{P}_{P1} & \mathbf{P}_{P2} & \cdots & \mathbf{P}_{PN} & \mathbf{P}_{P1}\left(\frac{j\omega_P/\zeta_1}{1+j\omega_P/\zeta_1}\right) & \mathbf{P}_{P2}\left(\frac{j\omega_P/\zeta_1}{1+j\omega_P/\zeta_1}\right) & \cdots & \mathbf{P}_{PN}\left(\frac{j\omega_P/\zeta_1}{1+j\omega_P/\zeta_1}\right) & \cdots & \mathbf{P}_{P1}\left(\frac{j\omega_P/\zeta_K}{1+j\omega_P/\zeta_K}\right) & \cdots & \mathbf{P}_{PN}\left(\frac{j\omega_P/\zeta_K}{1+j\omega_P/\zeta_K}\right) \end{bmatrix} \begin{bmatrix} M_{01} \\ M_{02} \\ \vdots \\ M_{0N} \\ M_{11} \\ M_{12} \\ \vdots \\ M_{1N} \\ \vdots \\ M_{K1} \\ \vdots \\ M_{KN} \end{bmatrix}$$

$$\mathcal{R}_p = \mathbf{A}_p M \tag{14}$$

The real and imaginary parts are separated, making the entire system real and ensuring a real answer. Multiple locations and/or orientations are included to get enough measurements to make it possible to solve for the parameters M_{kn}:

$$\begin{bmatrix} \mathrm{Re}(\mathcal{R}_P) \\ \mathrm{Im}(\mathcal{R}_P) \end{bmatrix} = \begin{bmatrix} \mathrm{Re}(\mathbf{A}_P) \\ \mathrm{Im}(\mathbf{A}_P) \end{bmatrix} \begin{bmatrix} M_{01} \\ M_{02} \\ \vdots \\ M_{0N} \\ M_{11} \\ M_{12} \\ \vdots \\ M_{1N} \\ \vdots \\ M_{K1} \\ \vdots \\ M_{KN} \end{bmatrix}. \tag{15}$$

Many of the parameters M_{kn} can be zero since not every relaxation will have all the tensor components and the non-zero values of M_{kn} will be positive. Since the parameters M_{kn} are non-negative, the function lsqnonneg in MATLAB which uses the algorithm found in [12] is used to solve (15).

5. RESULTS

Two targets were measured that are made with loops of wire so that their theoretical parameters are easily estimated to demonstrate the accuracy of the modeling technique. The first loop target is a simple loop of 22 AWG copper wire formed into a loop with a circumference of 10 cm, which has a theoretical relaxation frequency of 10.0 kHz. The theoretical and estimated model parameters are graphed as a function of the relaxation frequency, $f_r = \zeta/2\pi$, in Fig. 3 for

the single-loop target. The agreement between the theory and experiment is very good. Since the loop is z-directed, the theory predicts a single *z* component for the dipole expansion at 10.0 kHz; however, the expansion in equation (8) is used for this inversion which allows for three components. Ideally, the inversion would return exactly zero amplitudes for the additional components, but because of measurement errors, the additional components will not always have an amplitude of exactly zero. The additional components near 10.0 kHz are seen to very small in figure 3. These components could be easily due to a small misalignment of the target in the measurement system. Note that in the measured results, there is weak relaxation at 250 kHz that is not predicted theoretically, which we believe is due to the finite thickness of the wire that is not taken into account in the theoretical model.

The second loop target is the three-loop target shown in Fig. 1b with the theoretical model (3). The theoretical and estimated model parameters are shown in Table I and are graphed as a function of the relaxation frequency in Fig. 4 Each relaxation frequency for this target has a different component due to the arrangement of the loops. The agreement between the theory and experiment is very good even for this more complex target.

Results are shown in Figures 5 through 11 for a 1983 Lincoln penny, a nail, a 9 mm cartridge, a 0.45 caliber cartridge, a ferrite core, and two anti-personnel landmines. Some of these targets have been chosen for obvious familiarity while others were selected as representative examples of common landmines of interest. The parameters M_{0n} are due to the frequency independent magnetic permeability of the targets and are labeled as DC on the figures. These parameters are essentially zero for most of the targets since they are non-magnetic, but are non-zero for the steel nail, the ferrite core, and the two landmines since they are magnetic. All of the magnetic targets except for the ferrite core have relaxation terms, M_{kn}, in addition to the magnetic terms, M_{0n}. The experimental results for this broad range of targets demonstrate the capability of the model to represent the targets.

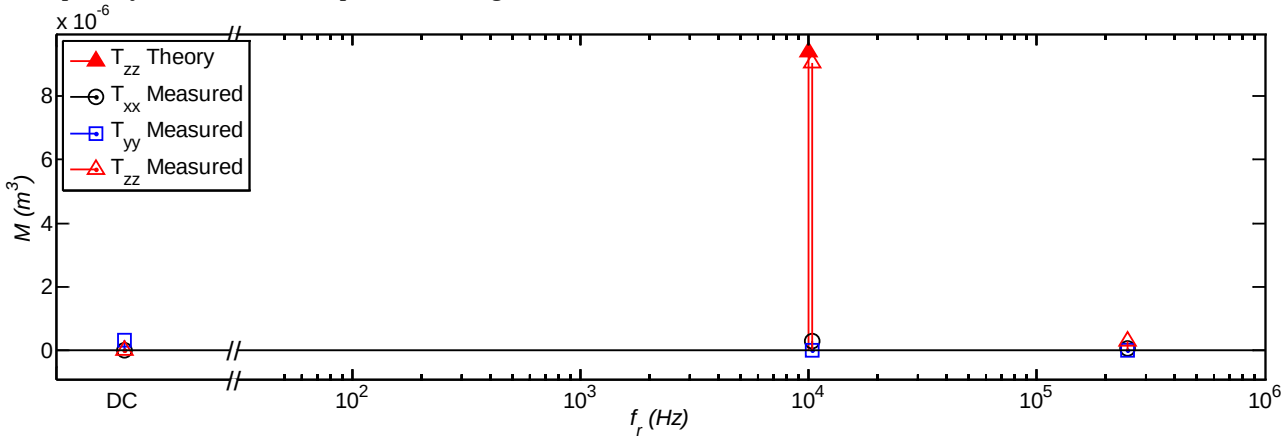

Fig. 3. Estimated and theoretical model parameters for the single-loop target as a function of relaxation frequency.

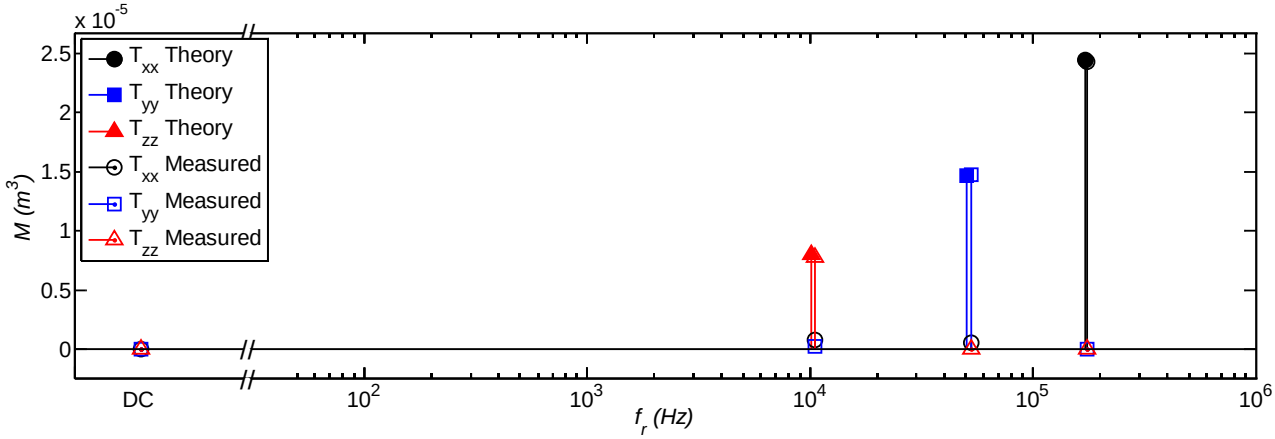

Fig. 4. Estimated and theoretical model parameters for the three-loop target as a function of relaxation frequency.

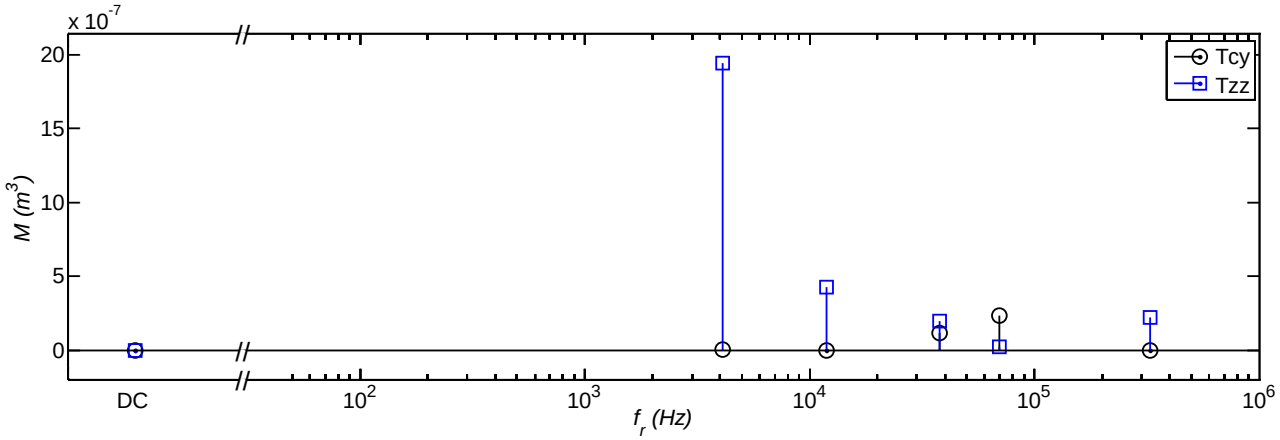

Fig. 5. Estimated model parameters for 1983 U.S Lincoln Penny as a function of relaxation frequency.

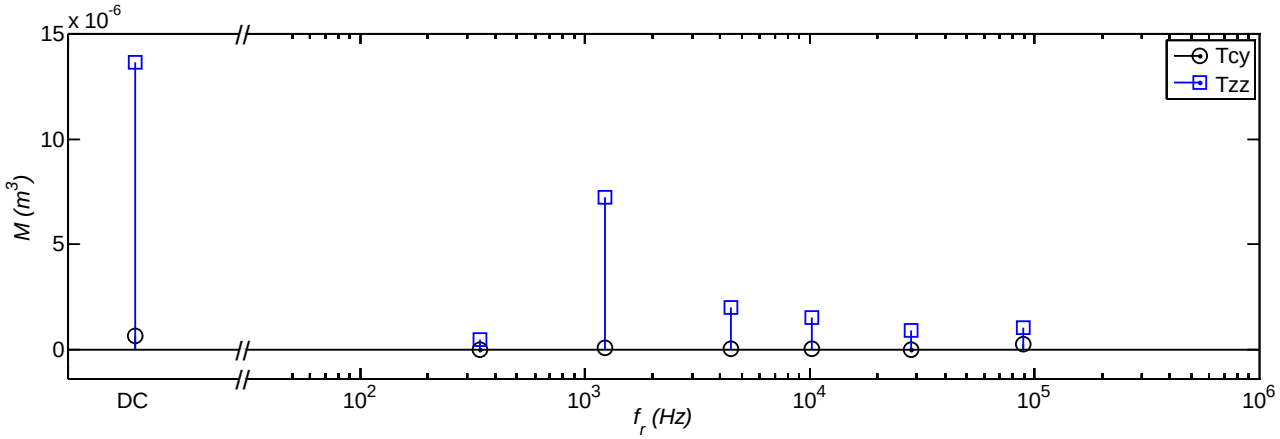

Fig. 6. Estimated model parameters for steel nail as a function of relaxation frequency.

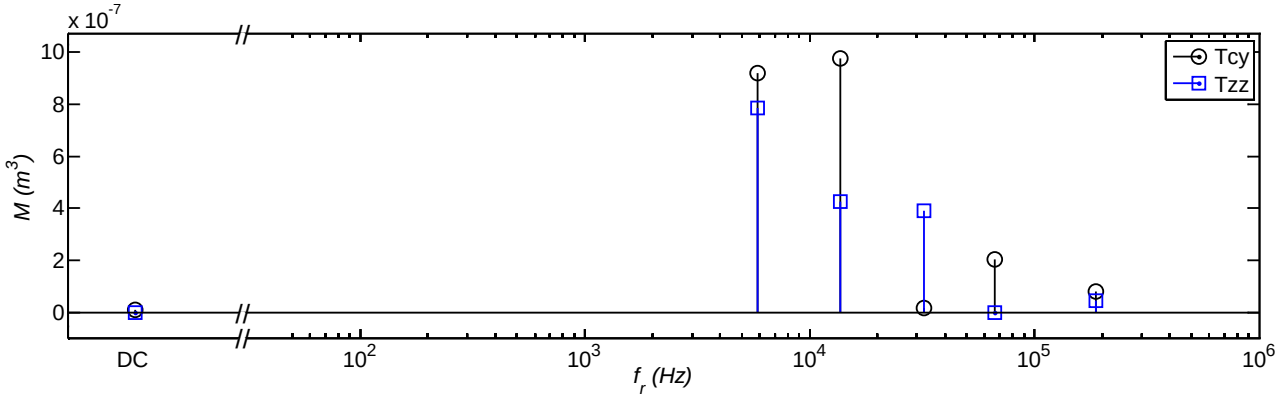

Fig. 7. Estimated model parameters for a 9mm NATO/Luger Cartridge as a function of relaxation frequency.

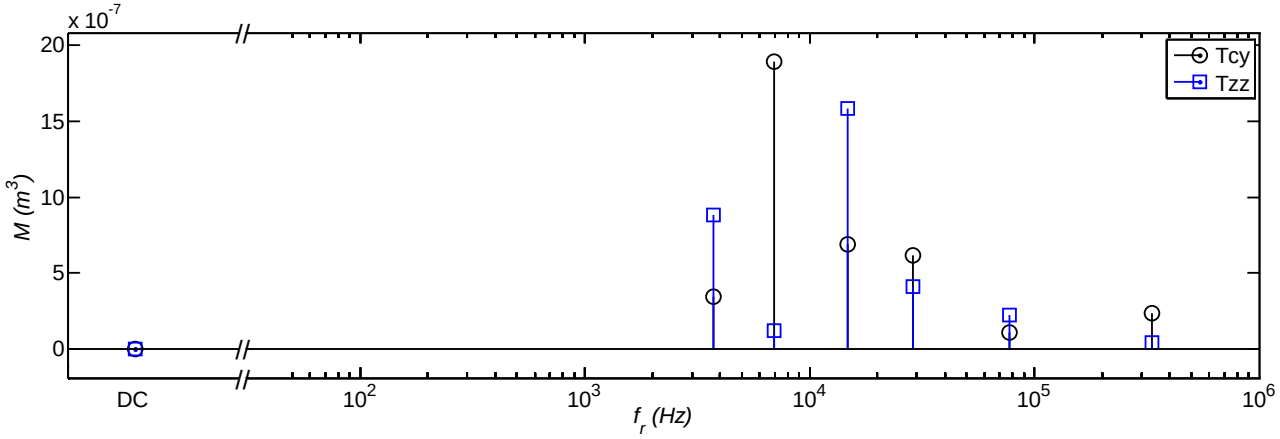

Fig. 8. Estimated model parameters for a 0.45caliber S&B Cartridge as a function of relaxation frequency.

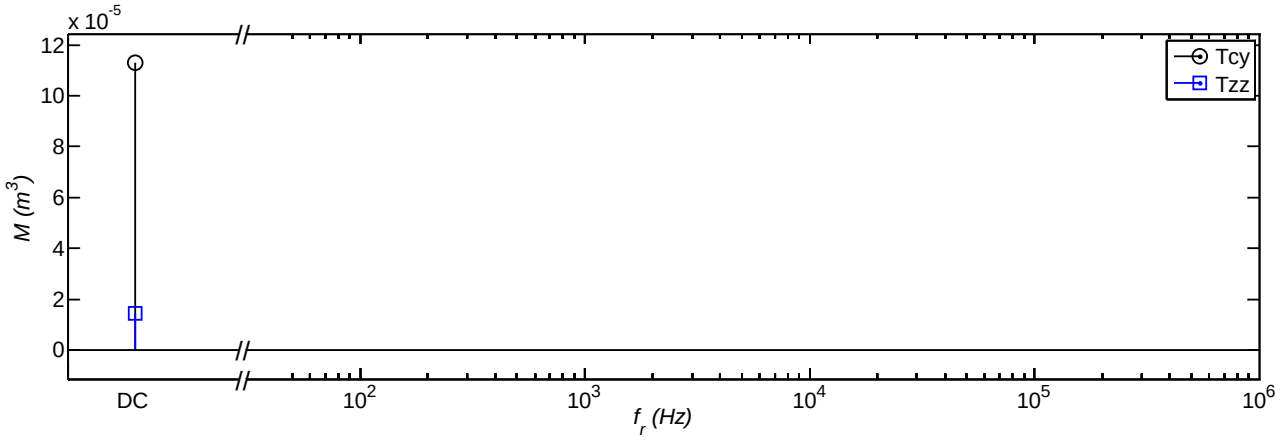

Fig. 9. Estimated model parameters for a Ferrite Core as a function of relaxation frequency.

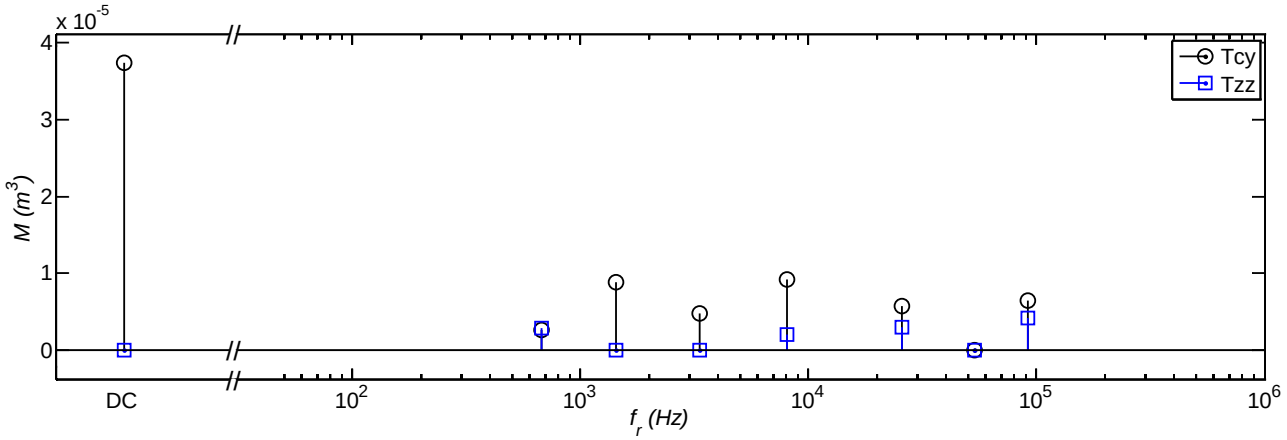

Fig. 10. Estimated model parameters for an anti-personnel medium-metal landmine as a function of relaxation frequency.

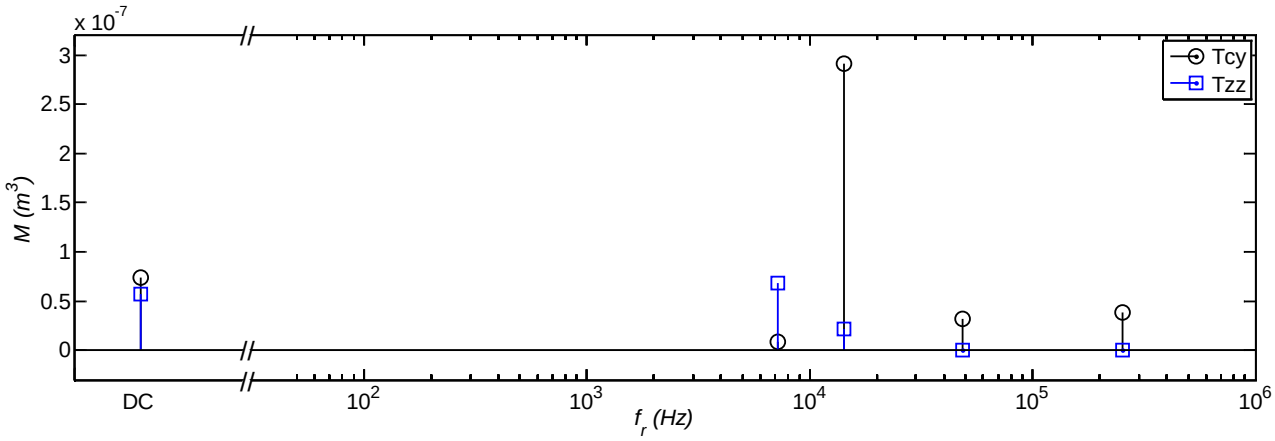

Fig. 11. Estimated model parameters for an anti-personnel low-metal landmine as a function of relaxation frequency.

6. CONCLUSIONS

An experimental facility has been established to measure the response of typical targets for EMI sensors as a function of location and orientation. A method of modeling the targets as an expansion of simple dipoles with discrete relaxations is presented along with a method to invert the measured responses to obtain the model parameters. The models are valid for any position and orientation of the target. Targets with known models were measured to establish the accuracy of the technique. Numerous other targets have been measured and their models catalogued. It is envisioned that the models derived in this work will be utilized in detection algorithms to reduce false alarm rates and increase the probability of detection for EMI sensors.

ACKNOWLEDGMENTS

This work is supported in part by the US Army Night Vision and Electronic Sensors Directorate, Science and Technology Division, Countermine Branch and in part by the U. S. Army Research Office under Contract Number W911NF-05-1-0257.

REFERENCES

[1] G. D. Sower and S. P. Cave, "Detection and identification of mines from natural magnetic and electromagnetic resonances," in *Proc. of SPIE 2496*, Orlando, FL, USA, 1995, pp. 1015-1024.

[2] C. E. Baum, "Detection and identification of mines from natural magnetic and electromagnetic resonances," in *Detection and identification of visually oscured targets*, C. E. Baum, Ed., ed Philadelphia: Talor and Francis, 1999, pp. 163-218.

[3] L. Collins, *et al.*, "An improved Bayesian decision theoretic approach for land mine detection," *Geoscience and Remote Sensing, IEEE Transactions on*, vol. 37, pp. 811-819, 1999.

[4] G. Ping, *et al.*, "Classification of landmine-like metal targets using wideband electromagnetic induction," *Geoscience and Remote Sensing, IEEE Transactions on*, vol. 38, pp. 1352-1361, 2000.

[5] E. B. Fails, *et al.*, "Performance of a four parameter model for modeling landmine signatures in frequency domain wideband electromagnetic induction detection systems," in *Proc. of the SPIE 6553*, 2007.

[6] S. E. Yuksel, *et al.*, "Hierarchical Methods for Landmine Detection with Wideband Electro-Magnetic Induction and Ground Penetrating Radar Multi-Sensor Systems," in *Geoscience and Remote Sensing Symposium, 2008. IGARSS 2008. IEEE International*, 2008, pp. II-177-II-180.

[7] G. D. Larson and J. Waymond R. Scott, "Automated, non-metallic measurement facility for testing and development of electromagnetic induction sensors for landmine detection," in *Proc. of the SPIE 7303*, 2009.

[8] W. R. Scott, "Broadband Array of Electromagnetic Induction Sensors for Detecting Buried Landmines," in *Geoscience and Remote Sensing Symposium, 2008. IGARSS 2008. IEEE International*, 2008, pp. II-375-II-378.
[9] H. Vesselle and R. E. Collin, "The signal-to-noise ratio of nuclear magnetic resonance surface coils and application to a lossy dielectric cylinder model. I. Theory," *Biomedical Engineering, IEEE Transactions on*, vol. 42, pp. 497-506, 1995.
[10] K. F. Casey and B. A. Baertlein, "An overview of Electromagnetic methods in subsurface detection," in *Detection and identification of visually oscured targets*, C. E. Baum, Ed., ed Philadelphia: Talor and Francis, 1999, pp. 9-46.
[11] G. Arfken, *Mathematical Methods for Physicists*, Second ed. San Diego, CA: Academic Press, 1985.
[12] M. H. Wei, *et al.*, "Robust Estimation of the Discrete Spectrum of Relaxations for Electromagnetic Induction Responses," *Geoscience and Remote Sensing, IEEE Transactions on*, vol. 48, pp. 1169-1179, 2010.
[13] C. E. Baum, "The magnetic polarizability dyadic and point symmetry," in *Detection and identification of visually oscured targets*, C. E. Baum, Ed., ed Philadelphia: Talor and Francis, 1999, pp. 219-242.